Activating transcription factor 4 regulates stearate-induced vascular calcification

Masashi Masuda,* Tabitha C. Ting,* Moshe Levi,* Sommer J. Saunders,* Shinobu Miyazaki-Anzai,* and Makoto Miyazaki[1,*,†]

Division of Renal Diseases and Hypertension* and Division of Endocrinology, Diabetes, and Metabolism,† University of Colorado Denver, Aurora, CO

Abstract Previously, we reported that stearate, a saturated fatty acid, promotes osteoblastic differentiation and mineralization of vascular smooth muscle cells (VSMC). In this study, we examined the molecular mechanisms by which stearate promotes vascular calcification. ATF4 is a pivotal transcription factor in osteoblastogenesis and endoplasmic reticulum (ER) stress. Increased stearate by either supplementation of exogenous stearic acid or inhibition of stearoyl-CoA desaturase (SCD) by CAY10566 induced ATF4 mRNA, phosphorylated ATF4 protein, and total ATF4 protein. Induction occurred through activation of the PERK-eIF2α pathway, along with increased osteoblastic differentiation and mineralization of VSMCs. Either stearate or the SCD inhibitor but not oleate or other fatty acid treatments also increased ER stress as determined by the expression of p-eIF2α, CHOP, and the spliced form of XBP-1, which were directly correlated with ER stearate levels. ATF4 knockdown by lentiviral ATF4 shRNA blocked osteoblastic differentiation and mineralization induced by stearate and SCD inhibition. Conversely, treatment of VSMCs with an adenovirus containing ATF4 induced vascular calcification. Our results demonstrated that activation of ATF4 mediates vascular calcification induced by stearate.—Masuda, M., T. C. Ting, M. Levi, S. J. Saunders, S. Miyazaki-Anzai, and M. Miyazaki. **Activating transcription factor 4 regulates stearate-induced vascular calcification. *J. Lipid Res.* 2012.** 53: **1543–1552.**

Supplementary key words stearoyl-CoA desaturase • endoplasmic reticulum • fatty acid/desaturases • fatty acid/metabolism • smooth muscle cells • vascular biology

Cardiovascular disease, such as vascular calcification, is the leading cause of death in patients with chronic kidney disease, accounting for over 50% of deaths (1, 2). Vascular calcification is frequently observed in advanced atherosclerotic lesions and is a highly regulated process that recapitulates osteogenesis in bone formation. Recent in vivo and in vitro studies have implicated the involvement of numerous positive and negative regulators, including serum phosphate, several lipid-derived molecules (saturated fatty acids, oxysterol, and oxidized phospholipids), and hormonal factors (tumor necrosis factor-α, bone morphogenetic protein-2, matrix gla protein, osteocalcin, fibroblast growth factors, and Klotho) in the pathogenesis of vascular calcification (3–10).

Recently, we reported that bile acid nuclear receptor, farnesoid X receptor (FXR), and oxysterol nuclear receptor, liver X receptor (LXR), elicit opposite effects on vascular calcification (11–13). We found that FXR activation attenuated CKD-dependent atherosclerotic calcification in ApoE$^{-/-}$ mice with 5/6 nephrectomy. FXR activation by either VP16-FXR overexpression or INT-747 (an FXR-specific agonist) treatment attenuated mineralization of vascular smooth muscle cells (VSMCs) in culture. Conversely, FXR inhibition by FXR shRNA and the dominant negative (DN) form of FXR augmented vascular calcification (11). In contrast to FXR, LXR activation by LXR agonists and adenovirus-mediated LXR overexpression by VP16-LXRα and VP16-LXRβ promoted mineralization of VSMCs. Conversely, LXR inhibition by dominant negative forms of LXRα and LXRβ attenuated vascular calcification in VSMCs (12). The regulation of mineralization by FXR and LXR agonists was highly correlated with changes in lipid accumulation, fatty acid synthesis, and the expression of sterol regulatory element binding protein-1 (SREBP-1). The rate of lipogenesis in VSMCs through the SREBP-1c-dependent pathway was reduced by FXR activation but increased by LXR activation (11, 12). SREBP-1c overexpression promoted mineralization in VSMCs, whereas SREBP-1c DN inhibited alkaline phosphatase activity and mineralization induced by LXR agonists. LXR and SREBP-1c activations increased, whereas FXR activation decreased saturated and monounsaturated fatty acids derived from lipogenesis. Furthermore, we found that stearate markedly

This work was supported in part by American Heart Association Grant 10BGIA458005 and 12BGIA11380005 to Dr. Miyazaki.

Manuscript received 4 May 2012 and in revised form 18 May 2012.

Published, JLR Papers in Press, May 25, 2012
DOI 10.1194/jlr.M025981

Abbreviations: ALP, alkaline phosphatase; ATF4, activating transcription factor 4; CHOP, C/EBP homologous protein; eIF2α, α-subunit of eukaryotic initiation factor 2; ER, endoplasmic reticulum; FXR, farnesoid X receptor; LXR, liver X receptor; nx, nephrectomy; MOI, multiplicity of infection; OCN, osteocalcin; OPG, osteoprotegerin; p-, phosphorylated; PERK, PKR-like endoplasmic reticulum kinase; SCD, stearoyl-CoA desaturase; SREBP-1; sterol regulatory element binding protein-1; UPR, unfolded protein response; VSMC, vascular smooth muscle cell; XBP, X-box binding protein.

[1]To whom correspondence should be addressed.
e-mail: Makoto.Miyazaki@ucdenver.edu

promoted mineralization of VSMCs compared with other fatty acids. Inhibition of acetyl-CoA carboxylase or acyl-CoA synthetase reduced mineralization of VSMCs, whereas inhibition of stearoyl-CoA desaturase (which converts stearate to oleate) promoted mineralization and osteoblastic differentiation (12). We also found that increased cholesterol synthesis and uptake by LXR and SREBP-1c activations contributed to vascular calcification (13). Therefore, we concluded that a stearate metabolite derived from lipogenesis promotes vascular calcification. However, the molecular mechanism by which stearate metabolites promote osteoblastic differentiation and mineralization of VSMCs remains elusive.

The endoplasmic reticulum (ER) is a major site for the regulation of calcium and lipid homeostasis. ER stress (also known as the unfolded protein response, UPR) is an integrated signal transduction pathway involved in the localization and folding of secreted and transmembrane proteins. A number of cellular stress conditions lead to the accumulation of unfolded or misfolded proteins in the ER lumen. The UPR is initiated by activation of three molecules: PKR-like endoplasmic reticulum kinase (PERK), inositol-requiring enzyme 1 (IRE1), and activating transcription factor 6 (ATF6) (14, 15). Activation of PERK leads to the phosphorylation of the α-subunit of eukaryotic initiation factor 2 (eIF2α), which inhibits the assembly of the 80S ribosome and inhibits protein synthesis (16, 17). In contrast to most proteins, activating transcription factor 4 (ATF4) is not affected by the translational attenuation of eIF2α phosphorylation because ATF4 has two small upstream open reading frames in its 5′-untranslated region. These upstream open reading frames, which prevent translation of the true ATF4 under normal conditions, are bypassed only when eIF2α is phosphorylated, and thereby permit ATF4 translation (16, 18). ATF4 is a pivotal transcription factor that mediates not only ER stress but also osteoblastic differentiation (18, 19). The transcriptional activity of ATF4 is regulated through post-translational phosphorylation by ribosomal S6 kinase 2 (RSK2) and PKA (18–20). In addition to ER stress markers, such as ATF3 and C/EBP homologous protein (CHOP), transcriptional targets of ATF4 include osteocalcin, an osteoblast-specific marker for the late stage of osteoblast differentiation (18), and osterix, another essential transcription factor in osteoblast differentiation (18, 20–22). ATF4 is also required for preserving mature osteoblast functions, including the synthesis of collagen, the most abundant extracellular protein found in bones and calcified vasculatures (18). It has recently been reported that ER stress mediated via the PERK-eIF2α-ATF4 pathway is involved in osteoblast differentiation induced by bone morphogenetic protein-2 (23). However, the role of ATF4 in the regulation of vascular calcification and vascular osteogenesis has yet to be determined.

MATERIALS AND METHODS

Cell culture studies

MOVAS-1 cells were kindly provided by Dr. Husain at the University of Toronto and cultured in DMEM containing 10% FBS with either 3.0 mM phosphate or 5.0 mM glycerophosphate (24, 25). MOVAS-1 cells were treated with triacsin C (Enzo Life Sciences) and free fatty acid-BSA complexes. The fatty acid-BSA complexes were generated as previously described (12, 26). The medium was changed every 2–3 days. Seven days after reaching confluence, the cells were stained with Alizarin red to identify calcium deposits.

Calcium content in cultured cells

Calcium deposition in the plates was quantified as previously described (11). Cells were decalcified using a 0.6 M HCl solution. After collecting the supernatant, the cells were washed with PBS and solubilized with a 0.1 N NaOH/0.1% SDS solution for protein quantification. Calcium content was quantified calorimetrically using the o-cresolphthalein method. Protein content was measured using a BCA protein assay kit.

RNA analysis

Total RNA was isolated using Tri reagent in conjunction with an RNAeasy kit. Real-time quantitative PCR assays were performed by using an Applied Biosystems StepOne qPCR instrument. In brief, 1 μg of total RNA was reverse transcribed with random hexamers by using the High Quality Reverse Transcription Reagents Kit (Applied Biosystems). Each amplification mixture (10 μl) contained 25 ng cDNA, 900 nM forward primer, 900 nM reverse primer, and 5 μl of Universal Fast PCR Master Mix. The quantification of given genes was expressed as the mRNA level normalized to a ribosomal housekeeping gene (18S or 36B4) using the ΔΔCt method. Primer sequences are available upon request. The spliced form of X-box binding protein-1 (XBP-1) was analyzed by RT-PCR coupled with PstI digestion, as described previously (27).

Adenoviral transduction for MOVAS-1 cells

MOVAS-1 cells were infected with recombinant adenoviruses at a multiplicity of infection (MOI) of 40. An adenovirus expressing ATF4 was generated using the ViraPower Adenovirus Expression System (Invitrogen). MOVAS-1 cells were infected with the adenovirus in DMEM with 10% FBS. After 6 h, the infected cells were treated with fresh media for 7 days.

Generation of ATF4-, Elovl6-, and PERK-knockdown MOVAS-1 cells

MOVAS-1 cells were infected with recombinant lentiviruses expressing control shRNA, five ATF4 shRNAs (Open Biosystems clone IDs: TRCN0000071723, TRCN0000071724, TRCN0000071725, TRCN0000071726, TRCN0000071727), or six PERK shRNAs (Open Biosystems clone IDs: V2LMM_51300, V2LMM_46582, V2LMM_41655, V3LMM_516599, V3LMM_478942, V3LMM_478941), or six Elovl6 shRNAs (V2LMM_26975, V2LMM_23217, V3LMM_522399, V3LMM_522398, V3LMM_453014, V3LMM_453017). Colonies were selected by treatment with 5 μg/ml puromycin for 7 days. A single colony was isolated from MOVAS-1 cells infected with each lentivirus. MOVAS-1 cells infected with lentiviruses expressing ATF4 shRNA (TRCN0000071723), PERK shRNA (V3LMM_478941), and Elovl6 (V2LMM_23217) were used as ATF4-knockdown VSMCs, PERK-knockdown VSMCs, and Elovl6-knockdown VSMCs, respectively, unless otherwise indicated.

Western blotting

Cell and tissue lysates were prepared using RIPA buffer (Cell Signaling). The samples were separated by SDS-PAGE, transferred to a nitrocellulose membrane, and immunoblotted with an ATF4 antibody (Santa Cruz Biotechnology), CHOP antibody and GAPDH (Santa Cruz Biotechnology), and phospho-serine antibody (Millipore). Samples were visualized using horseradish peroxidase coupled to an anti-mouse secondary antibody, with enhancement by an ECL detection kit. For phosphorylated (p-)ATF4 detection, the

lysates were immunoprecipitated with an ATF4 antibody and immunoblotted using a phospho-serine antibody.

Stearate levels in ER

VSMC homogenate was centrifuged at 10,000 *g* twice to remove the large debris. The resulting supernatant was layered on a discontinuous sucrose gradient (2 ml of 30% sucrose and 4 ml of 38% sucrose prepared in 10 mM HEPES, pH 7.4) and subjected to centrifugation at 100,000 *g* for 2 h to obtain the ER, which precipitated. Total lipids from the ER fraction were isolated by Bligh and Dyer's method. Fatty acids were quantified using gas chromatography as previously described (28). Protein content was measured using a BCA protein assay kit.

Stearoyl-CoA desaturase activity

MOVAS-1 cells treated with CAY10566 were incubated with 200 μM stearate-BSA complex containing 1 μCi ^{14}C-stearate. Total lipids were saponified with 3 M sodium hydroxide/ethanol. The saponified fatty acids were separated by 10% silver nitrate-coated thin-layer chromatography. The ratio of the cpm in the band corresponding to oleic acid to the cpm in the band corresponding to stearate was used to calculate stearoyl-CoA desaturase (SCD) activity as previously described (28).

Alkaline phosphatase activity

Alkaline phosphatase (ALP) activity was measured using *p*-nitrophenyl phosphate as the substrate (29).

Statistical analysis

Data were collected from more than two independent experiments and were reported as the means ± SE. Statistical analysis for two-group comparison was performed using the Student *t*-test or one-way ANOVA with a Student-Newman posthoc test for multigroup comparison. Significance was accepted at $P < 0.05$.

RESULTS

Stearate treatment increases CHOP, phosphorylated ATF4 protein, and total ATF4 protein, associated with increased mineralization and osteoblastic differentiation of VSMCs

Stearate and palmitate treatment induced mineralization of mouse vascular smooth muscle cell line MOVAS-1, an immortalized cell line recently described as an in vitro model of vascular calcification (24). Similar to our previous observations, both stearate and palmitate increased calcium content by 4.3-fold and 2.4-fold, respectively, compared with no treatment (**Fig. 1A**) (12). Other fatty acids, such as palmitoleate, oleate, and vaccenate, did not affect mineralization of MOVAS-1 cells (Fig. 1A). The procalcific effect of stearate showed dose dependency (Fig. 1B). In addition, stearate treatment but not other fatty acid treatments significantly induced osteoblastic differentiation as assayed with ALP activity (Fig. 1C) and osteocalcin (OCN) gene expression (**Fig. 2B**).

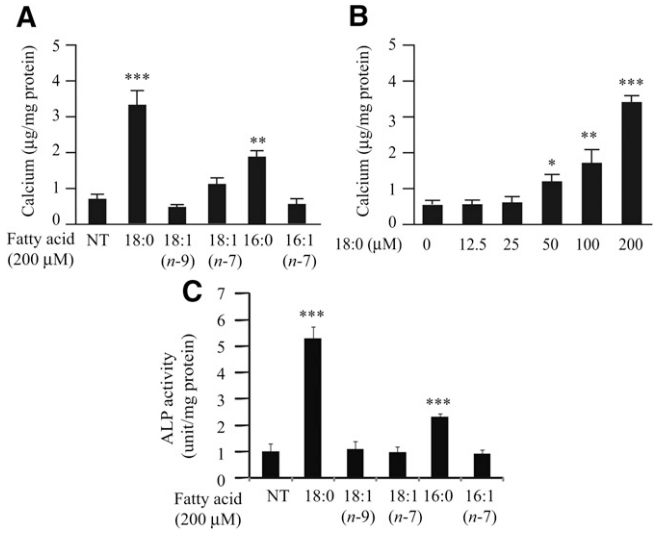

Fig. 1. Stearate induces mineralization in MOVAS-1 cells. (A–C) MOVAS-1 cells were treated with a fatty acid-BSA complex for 7 days in the presence of 5.0 mM glycerophosphate. (A) Calcium content in MOVAS-1 cells treated with the indicated fatty acids at 200 μM. (B) Calcium content in MOVAS-1 cells treated with various concentrations of stearate for 7 days. (C) ALP activity in MOVAS-1 cells treated with the indicated fatty acids at 200 μM.

We next examined whether treatment of MOVAS-1 cells with stearate or other fatty acids increases the expression of ATF4, a pivotal transcription factor not only in osteogenesis but also in ER stress. MOVAS-1 cells were treated with either 200 μM of stearate or another fatty acid, such as palmitate, palmitoleate, oleate, or vaccenate, for 6 h. Stearate treatment increased ATF4 protein and mRNA levels by 23.9-fold and 7.0-fold, respectively, compared with no treatment (Fig. 2A, B). Palmitate treatment also increased ATF4 protein levels, but the effect was weaker than it was with stearate treatment (Fig. 2C). Treatment of MOVAS-1 cells with unsaturated fatty acids, including

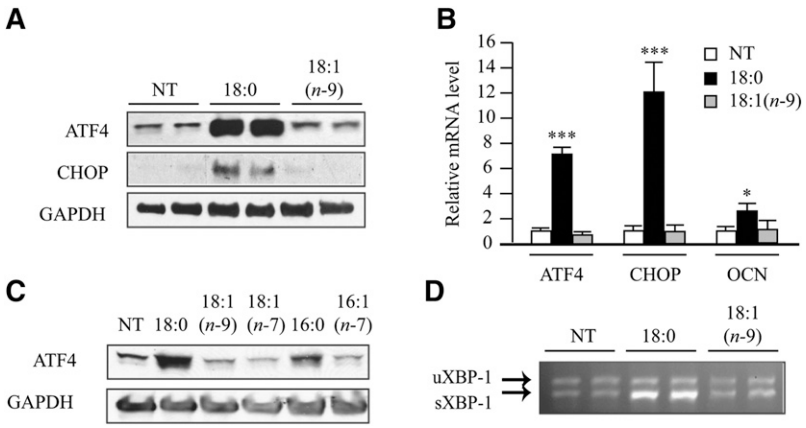

Fig. 2. Stearate induces ATF4 expression in MOVAS-1 cells. (A–D) MOVAS-1 cells were treated with the indicated fatty acids [palmitate (16:0), palmitoleate (16:1*n*-7), stearate (18:0), oleate (18:1*n*-9), and vaccenate (18:1*n*-7)] at 200 μM for 6 h (A) or 12 h (B and C) in the presence of 5.0 mM glycerophosphate. (A) ATF4 and CHOP protein were detected by immunoblot analysis with specific antibodies. GAPDH was used as a loading control. (B) ATF4, CHOP, and OCN mRNA. (C) ATF4 expression in MOVAS-1 cells treated with the indicated fatty acids at 200 μM for 12 h. (D) RT-PCR analysis of XBP-1 in MOVAS-1 cells. The upper band is the expression of unspliced forms of XBP-1 mRNA (uXBP-1) and the lower is the expression of spliced forms of XBP-1 mRNA (sXBP-1).

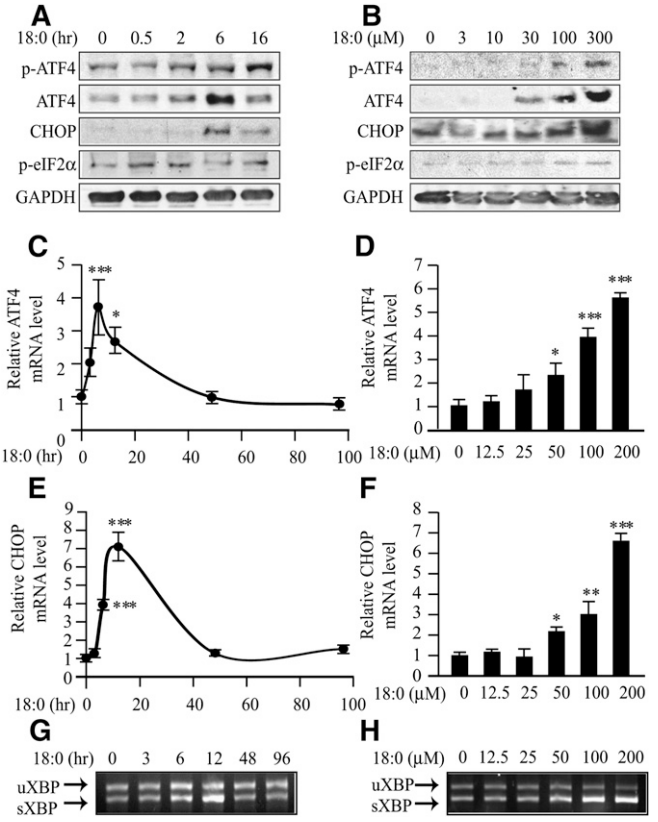

Fig. 3. Stearate induces unfolded protein response (ER stress) in MOVAS-1 cells. (A) Time-dependent effect of stearate on ATF4 expression. MOVAS-1 cells were treated with 200 μM stearate (18:0) and 5.0 mM glycerophosphate for various periods as indicated. Phosphorylated-ATF4 (p-ATF4), total ATF4 (ATF4), CHOP, and phosphorylated eIF2α (p-eIF2α) protein were detected by immunoblot analysis with specific antibodies. GAPDH was used as a loading control. (B) Dose-dependent effect of stearate. MOVAS-1 cells were treated with different concentrations of stearate (18:0) for 6 h. (C and D) ATF4 mRNA. (E and F) CHOP mRNA was analyzed with RT-qPCR analysis. (G and H) RT-PCR analysis of XBP-1 in MOVAS-1 cells. (C, E, and G) MOVAS-1 cells were treated with 200 μM stearate (18:0) for the indicated periods (0, 3, 6, 12, 48, and 96 h). (D, F, and H) MOVAS-1 cells were treated with various concentrations of stearate (18:0) for 12 h. (G and H) The PCR products were digested with PstI. The upper band is the expression of unspliced forms of XBP-1 mRNA (uXBP-1), and the lower is the expression of spliced forms of XBP-1 mRNA (sXBP-1). $*P < 0.05$, $**P < 0.01$, $***P < 0.001$.

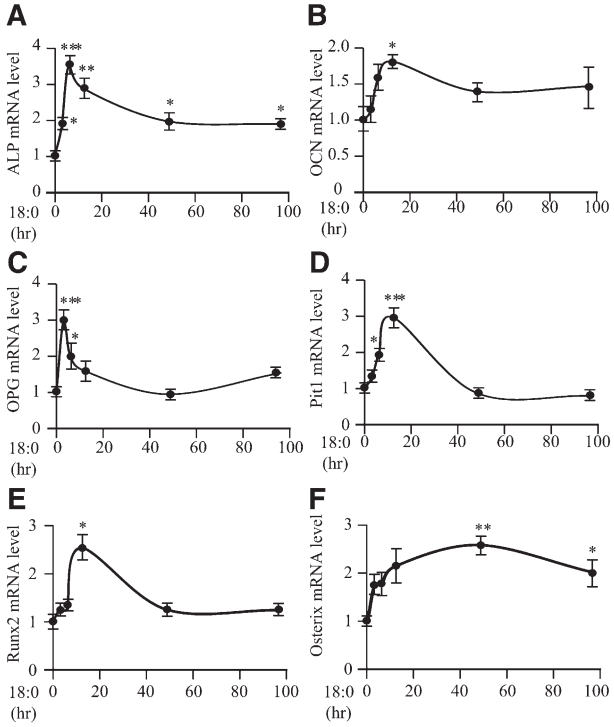

Fig. 4. Stearate induces gene expression of osteogenic transcription factors and markers. MOVAS-1 cells were treated with 200 μM stearate (18:0) for the indicated periods (0, 3, 6, 12, 48, and 96 h). (A–F) ALP (A), OCN (B), OPG (C), Pit1 (D), Runx2 (E), and Osterix (F) gene expression in MOVAS-1 cells. $*P < 0.05$, $**P < 0.01$, $***P < 0.001$.

oleate, palmitoleate, and vaccenate, did not affect ATF4 protein and mRNA levels (Fig. 2A–C). Consistently, mRNA and protein expression of CHOP, a major ATF4 target, were highly induced by stearate treatment but not oleate treatment (Fig. 2A, B). Levels of GAPDH protein used as a loading control did not vary between stearate and oleate treatment. In addition, stearate treatment caused a 3.3-fold increase in mRNA levels of the spliced form of X-box binding protein-1 (sXBP-1), another common marker of ER stress (Fig. 2D). The unspliced form of XBP-1 (uXBP-1) remained unchanged in MOVAS-1 cells treated with stearate (Fig. 2D). We also examined time- and dose-dependent effects of stearate on the expression of p-ATF4, which is an active form of ATF4 in osteoblastic differentiation. MOVAS-1 cells were treated with 200 μM stearate for up to 16 h. Phosphorylated ATF4 levels continuously increased compared with no treatment (time 0), whereas total ATF4 protein levels transiently increased up to 2.9-fold after 6 h of stearate treatment (**Fig. 3A**). We also examined whether PERK-eIF2α signaling contributed to the induction of ATF4 expression. Phosphorylated eIF2α levels were quickly and transiently induced between 0.5 and 2 h of treatment prior to the induction of ATF4 expression. CHOP protein was induced by 35.6-fold after 6 h of treatment (Fig. 3A). The effect of stearate on p-ATF4, total ATF4, CHOP, and p-eIF2α protein expression exhibited dose dependency (Fig. 3B). At a 200 μM concentration, 12 h stearate treatment induced ATF4, CHOP, and sXBP-1 mRNA expression by 3.8-fold, 7.1-fold, and 2.7-fold, respectively (Fig. 3C, E, G). Consistent with protein expression, the mRNA levels of ATF4, CHOP, and sXBP-1 continuously increased with 6 h of stearate treatment in a dose-dependent manner (Fig. 3D, F, H). The expressions of ATF4, CHOP, and sXBP-1 correlated with increases in calcium content of MOVAS-1 cells by stearate treatment (Figs. 1 and 3). Similar to the expression of genes involved in ER stress, stearate treatment induced several osteogenic markers, including ALP, OCN, osteoprotegerin (OPG), sodium-dependent phosphate transporter 1 (Pit1), Runx2, and Osterix with maximum induction at 6 h, 12 h, 3 h, 12 h, 12 h, and 48 h, respectively (**Fig. 4**).

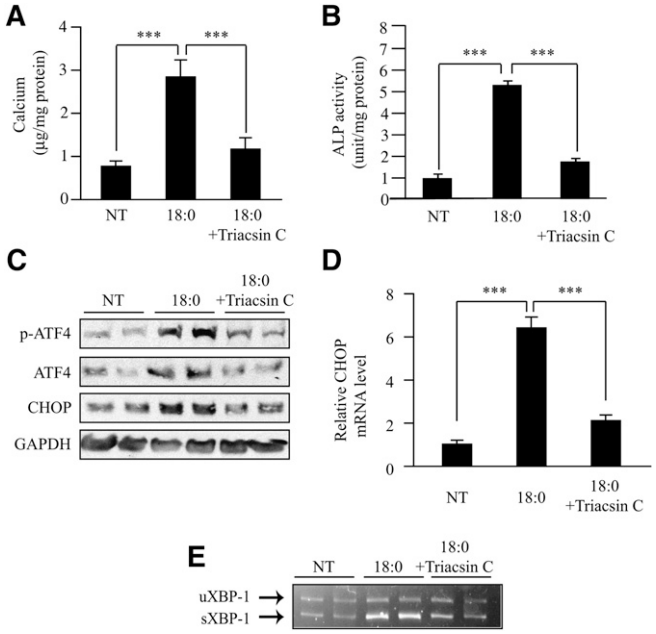

Fig. 5. Inhibition of acyl-CoA synthetase blocks mineralization and ER stress induced by stearate treatment. (A) Calcium content in MOVAS-1 cells treated with triacsin C (5 μM, acyl-CoA synthetase inhibitor) for 7 days in the presence of 200 μM stearate (18:0) and 5.0 mM glycerophosphate. (B) ALP activity. (C) MOVAS-1 cells were treated with 200 μM stearate for 10 h in the presence of 5 μM triacsin C. Phosphorylated ATF4 (p-ATF4), total ATF4 (ATF4), and CHOP protein were detected by immunoblot analysis with specific antibodies. GAPDH was used as a loading control. (D and E) MOVAS-1 cells were treated with triacsin C (5 μM) for 12 h in the presence of 200 μM stearate (18:0). (D) CHOP mRNA. (E) RT-PCR analysis of XBP-1 in MOVAS-1 cells. ***$P < 0.001$.

Alteration of stearate metabolism affects expression of ATF4 through the PERK-eIF2α pathway

To examine whether alteration of stearate metabolism affects ATF4 expression and ER stress, we used specific inhibitors triacsin C and CAY10566 to inhibit acyl-CoA synthetase and stearoyl-CoA desaturase, two major enzymes in stearate metabolism. MOVAS-1 cells were cotreated with stearate (200 μM) and triacsin C (5 μM). Corresponding with the effect of triacsin C on mineralization and osteoblastic differentiation (**Fig. 5A**, B), triacsin C treatment drastically reduced the expression of p-ATF4 and total ATF4 protein (Fig. 5C), CHOP protein and mRNA (Fig. 5C, D), and sXBP-1 mRNA (Fig. 5E).

Treatment with specific SCD inhibitor CAY10566 dose-dependently reduced SCD activity in MOVAS-1 cells (**Fig. 6A**), resulting in a significant increase in ER stearate levels (Fig. 6B). SCD inhibition by CAY10566 treatment induced mineralization (Fig. 6C) and osteoblastic differentiation (Figs. 6D and **7G**, H) of MOVAS-1 cells. Along with induction of vascular calcification, CAY10566 dose-dependently induced total ATF4, p-ATF4, and p-eIF2α protein expression (Fig. 6E). ATF4 mRNA, CHOP protein, CHOP mRNA, and sXBP-1 mRNA levels were also highly and dose-dependently induced by CAY10566 treatment (Figs. 6 and 7). ER stress and mineralization induced by CAY10566 were negatively correlated with SCD1 activity. Even in concentrations as low as 10 nM, CAY10566 induced CHOP mRNA expression, indicating that CAY10566 is as potent as other common inducers of ER stress, such as thapsigargin and tunicamycin, which also induce vascular calcification and ATF4 expression (Fig. 7C and data not shown). We also examined the time-dependent effect of CAY10566 on the expression of ATF4 and other ER stress markers. CAY10566 treatment transiently induced p-ATF4 expression. After 2 h of treatment, p-ATF4 levels were increased by 2.9-fold. Total ATF4 and CHOP protein levels were time-dependently increased by 8.2-fold and 8.1-fold, respectively, at 16 h of treatment (Fig. 6F). Phosphorylated PERK levels were increased by 15.7-fold at 2 h of CAY10566 treatment, whereas p-eIF2α levels were transiently increased by 1.91-fold at 6 h of CAY10566 treatment (Fig. 6F). The expressions of ATF4, CHOP, and sXBP mRNA were induced up to 96 h of 300 nM CAY10566 treatment (Fig. 7B, D, F). Corresponding with increased ATF4 expression, CAY10566 treatment significantly induced ALP, OCN, OPG, sodium-dependent phosphate transporter 1 (Pit-1), Runx2, and Osterix with maximum induction at 12 h, 48 h, 12 h, 48 h, 12 h, and 96 h of the treatment, respectively (Fig. 7G, H and data not shown).

To confirm whether SCD inhibition induces ATF4 and CHOP expression through the PERK-eIF2α pathway, we treated PERK-knockdown MOVAS-1 cells with 300 nM CAY10566 for 16 h. PERK knockdown completely inhibited the induction of ATF4 and CHOP protein induced by stearate (Fig. 6G).

In contrast to inhibition of SCD by CAY10566, SCD1 overexpression by an adenovirus system completely blocked mineralization of MOVAS-1 cells induced by stearate treatment (Fig. 6H). Treatment with adenoviruses containing SCD1 increased the expression of SCD1 by 5.3-fold (Fig. 6I), which was comparable to the induction of SCD1 by T0901317 treatment. The induction of total ATF4 and CHOP protein expression by stearate treatment was completely blocked by SCD overexpression (Fig. 6I).

Not only stearate but also palmitate induced ATF4 expression and mineralization (Figs. 1 and 2). We therefore hypothesized that the elongation of palmitate to stearate is required for palmitate-induced ATF4 induction and mineralization. To examine our hypothesis, we treated Elovl6-knockdown MOVAS-1 cells with palmitate (Fig. 6J). Elovl6 knockdown significantly reduced palmitate-induced ATF4 expression and mineralization (Fig. 6K, L).

ATF4 knockdown blocks mineralization and osteoblastic differentiation of VSMCs, whereas ATF4 overexpression induces vascular calcification

ATF4-knockdown MOVAS-1 cells were generated by treating MOVAS-1 cells with lentiviral shRNAs of ATF4. MOVAS-1 cells were infected with lentiviruses containing five different shRNAs for ATF4 or a control shRNA. The cells were treated with 5 μg/ml puromycin for 7 days to isolate colonies. Three shRNAs out of five effectively reduced ATF4 protein and mRNA expression (data not shown). In this study, we also used MOVAS-1 cells treated with a lentivirus generated by the clone

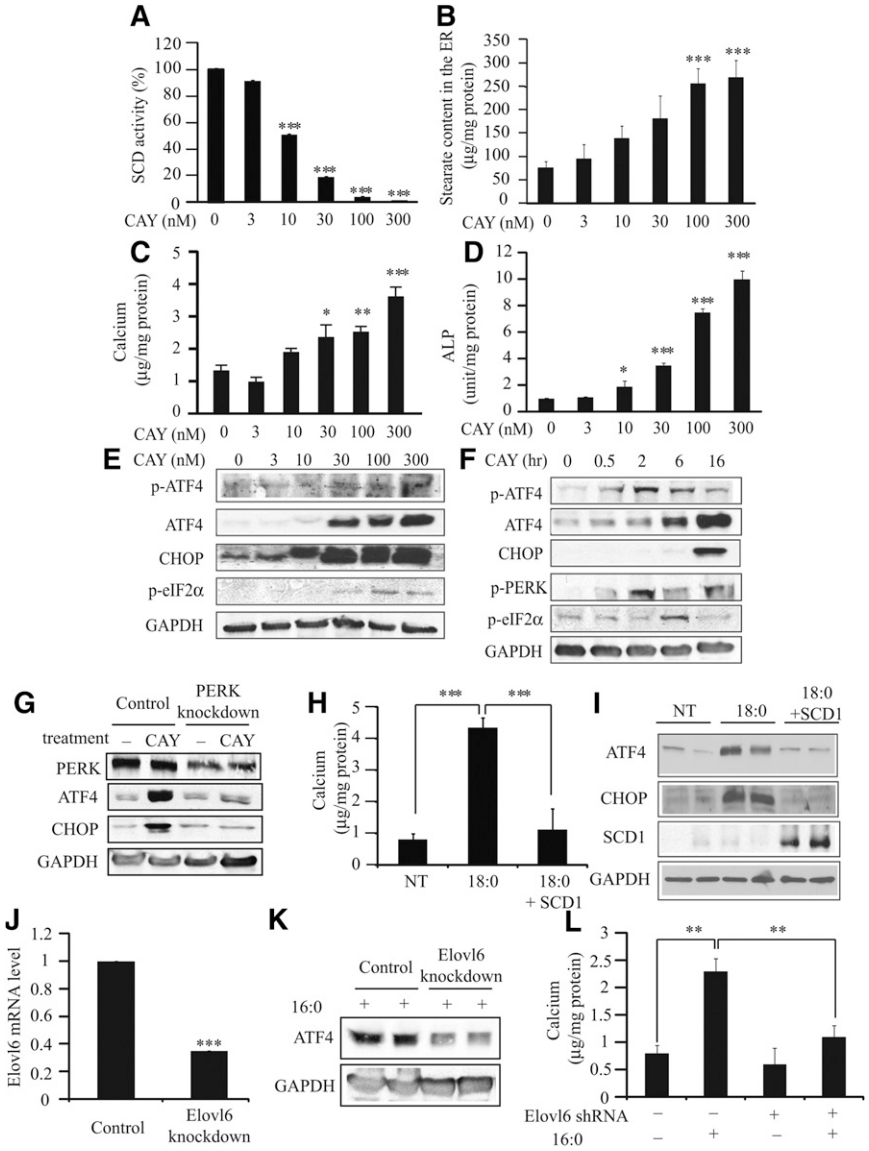

Fig. 6. SCD activity and ER stearate levels regulate ATF4 expression through PERK-eIF2α pathway, mineralization, and osteoblastic differentiation. MOVAS-1 cells were treated with different concentrations of CAY10566 (0, 3, 10, 30, 100, and 300 nM) for 16 h (A and B) or for 7 days in (C and D) in the presence of glycerophosphate. (A) SCD activity was measured using ^{14}C-stearic acid. (B) Stearate content in the ER was measured by GC. (C) Calcium content. (D) ALP activity. MOVAS-1 cells were treated with different concentrations of CAY10566. (E and F) ER stress. MOVAS-1 cells were treated with CAY10566 (SCD1 inhibitor) at the indicated times (0, 0.5, 2, 6, and 16 h) and concentrations (0, 3, 10, 30, 100, and 300 nM). Phosphorylated ATF4 (p-ATF4), total ATF4 (ATF4), CHOP, and phosphorylated eIF2α (p-eIF2α) proteins were detected by immunoblot analysis with specific antibodies. GAPDH was used as a loading control. (G) ATF4 and CHOP protein expression in PERK knockdown MOVAS-1 cells treated with CAY10566. PERK-knockdown MOVAS-1 cells were treated with 300 nM CAY10566 for 16 h. (H) Calcium content and (I) ATF4 and CHOP expression in MOVAS-1 cells treated with an adenovirus containing SCD1. MOVAS-1 cells were treated with an adenovirus containing SCD1 at a MOI of 40 for 3 h and then incubated for 7 days (H) or 8 h (I) in the presence of 200 μM stearate (18:0) and 5.0 mM glycerophosphate. (J) Elovl6 mRNA expression, (K) ATF4 protein expression, and (L) calcium content in Elovl6-knockdown MOVAS-1 cells. Elovl6-knockdown MOVAS-1 cells were treated with 200 μM palmitate (16:0) and 5.0 mM glycerophosphate for 6 h (J) and 7 days (K). $^{*}P < 0.05$, $^{**}P < 0.01$, $^{***}P < 0.001$ versus no treatment.

TRCN0000071723 as ATF4-knockdown MOVAS-1 cells, and the results are shown in **Fig. 8**. ATF4-knockdown MOVAS-1 cells and the control MOVAS-1 cells were treated with either stearate or CAY10566 for 7 days. ATF4 knockdown reduced mineralization and osteoblastic differentiation by 53% and 59% under basal conditions (Fig. 8A, B). In addition, ATF4 knockdown significantly attenuated stearate- and CAY10566-induced mineralization and ALP activity (Fig. 8A, B). Consistently, Alizarin staining showed that ATF4 knockdown markedly attenuated mineralization

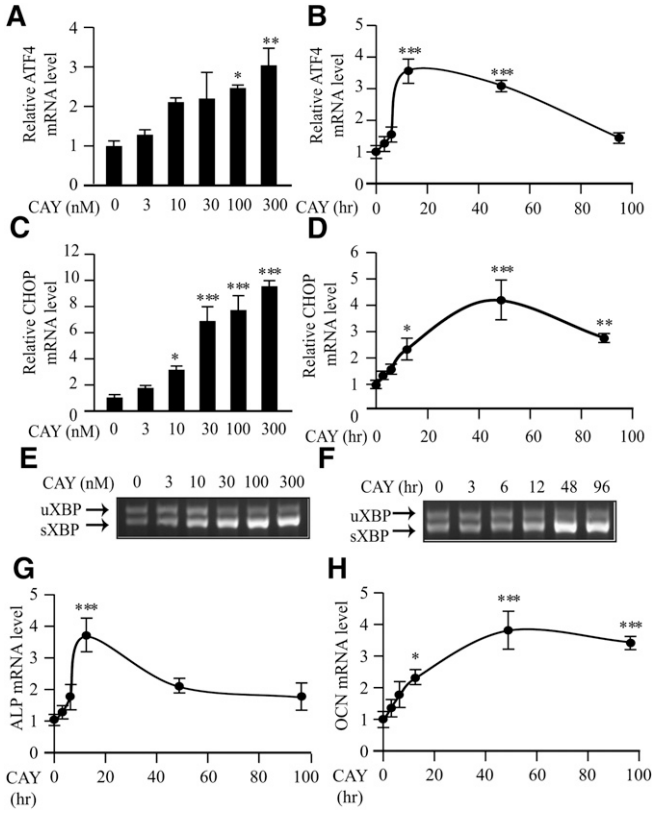

Fig. 7. SCD inhibition induces the expression of ER stress and osteogenic markers. (A and B) ATF4 mRNA. (C and D) CHOP mRNA. (E and F) RT-PCR analysis of XBP-1 in MOVAS-1 cells treated with CAY10566 in the presence of 5.0 mM glycerolphosphate. The upper band is the expression of unspliced forms of XBP-1 mRNA (uXBP-1), and the lower is the expression of spliced forms of XBP-1 mRNA (sXBP-1). (G) ALP mRNA and (H) OCN mRNA. (A, C, and E) mRNA levels were analyzed at 24 h of CAY10566 treatment. (B, D, F, G, and H) CAY10566 was used at 300 nM.

of MOVAS-1 cells induced by CAY10566 (Fig. 8C). As expected, ATF4 knockdown attenuated the induction of p-ATF4 and total ATF4 protein expression induced by CAY10566 (Fig. 8D) or stearate treatment (data not shown), resulting in the reduction of p-ATF4 and CHOP protein expression. Consistent with the immunoblot analysis, qPCR analysis showed that ATF4 deficiency alleviated the expression of ER stress markers [ATF3, asparagine synthetase (ASNS), CHOP, GADD34, and GRP78] and osteogenic markers (ALP, OCN, and Pit1) induced by CAY10566 treatment (Fig. 8E). Consistent results were obtained in ATF4-knockdown MOVAS-1 cells by a lentivirus derived from a different clone TRCN0000071724 (data not shown). In contrast to shRNA-mediated knockdown of ATF4, ATF4 overexpression mediated by the adenovirus (Ad) expression system induced mineralization and osteoblastic differentiation of MOVAS-1 cells. Although infection with Ad-ATF4 increased ATF4 expression by 4.3-fold (Fig. 8F), it was lower than ATF4 induction in MOVAS-1 cells treated with stearate (7.0-fold, shown in Fig. 2B). Calcium content, ALP activity, and OCN mRNA levels were increased by 3.9-, 4.5-, and 3.8-fold (Fig. 8G–I), respectively, in MOVAS-1 cells treated with Ad-ATF4 compared with MOVAS-1 cells treated with Ad-empty.

DISCUSSION

ATF4 is a critical transcription factor that mediates not only UPR/ER stress but also osteoblastic differentiation during bone formation (16, 18, 30–33). However, the role of ATF4 in vascular calcification and osteogenesis in the vasculature has not previously been determined. The results of our present study demonstrate, for the first time to our knowledge, that the activation and induction of ATF4 are key events in the pathogenesis of vascular calcification induced by stearate.

There are four reasons for using MOVAS-1 cells in this study, instead of the primary bovine calcifying vascular cells used in our previous studies (11, 12). First, MOVAS-1 cells have been established as a cell culture model of vascular calcification. Second, all of our previous observations in bovine calcifying vascular cells were perfectly replicated in MOVAS-1 cells. Third, mouse but not bovine lentiviral shRNAs are readily available from several commercial sources. Fourth, puromycin selection for the shRNA experiment significantly affects the growth, mineralization, osteoblastic differentiation, and morphology of primary vascular cells but not of MOVAS-1 cells.

We previously reported that stearate derived from SREBP-1-dependent de novo lipogenesis promotes vascular calcification of bovine aortic calcifying vascular cells (12). Stearate is one of the major saturated fatty acids in mammals and is acquired through two pathways: *i*) dietary fat absorption and *ii*) de novo lipogenesis. Although mammals obtain a large amount of stearate from their diets, stearate can also accumulate through de novo fatty acid synthesis. Consistent with our previous report using bovine cells (12), stearate most potently induced vascular osteoblastic differentiation and calcification in mouse aortic VSMCs. In a number of recent studies using cell culture systems, saturated fatty acids, including stearate, have been shown to exert lipotoxic effects via ER stress (34–37). We therefore hypothesized that the induction of ATF4 through an ER stress signaling pathway mediates stearate-induced vascular calcification and osteogenesis. Consistent with our hypothesis was our finding that stearate treatment drastically and dose-dependently induced p-eIF2α, ATF4, CHOP, and sXBP-1 expression. Phosphorylated eIF2α levels increased prior to the induction of ATF4 protein expression in response to stearate and CAY10566 treatment, suggesting that the translation of ATF4 is induced by the activation of eIF2α.

The effect of stearate on vascular calcification and ATF4 is specific compared with other fatty acids. Neither mineralization nor induction of proteins involved in ER stress (ATF4, p-eIF2α, and CHOP) was detected in MOVAS-1 cells treated with oleate and other unsaturated fatty acids (Figs. 1 and 2). Although palmitate induced mineralization and ER stress in MOVAS-1 cells to a lesser extent than stearate, the induction of ATF4 expression by palmitate

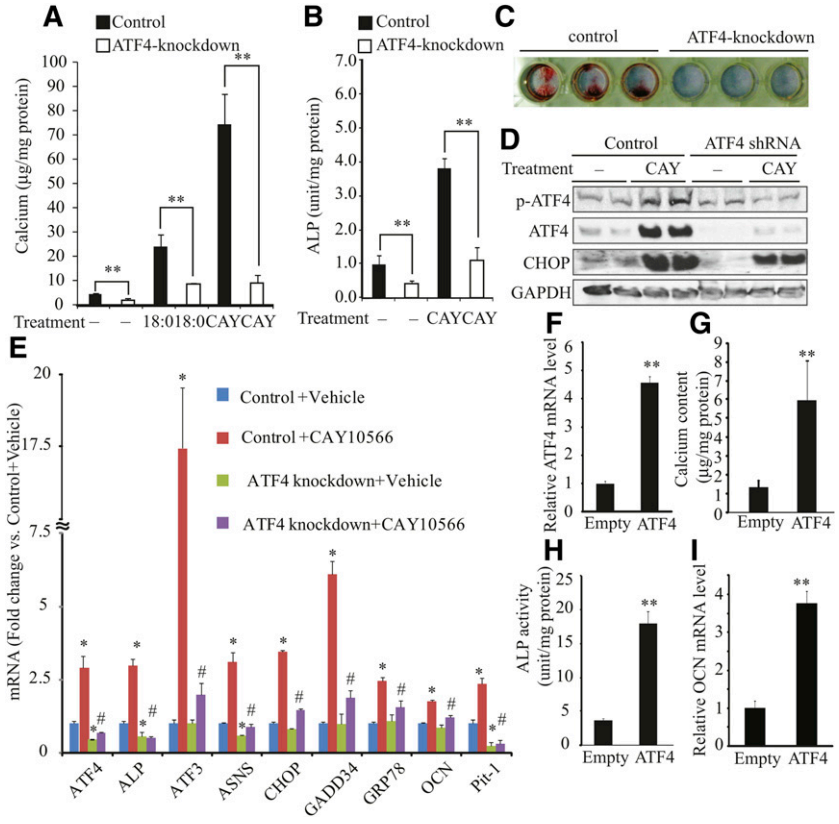

Fig. 8. ATF4 expression alters mineralization and osteoblastic differentiation of VSMCs induced by stearate and SCD inhibitor CAY10566. (A) Mineralization and (B) ALP activity of ATF4-knockdown MOVAS-1 cells treated with stearate (200 μM) and CAY10566 (300 nM) for 7 days in the presence of high-phosphate (3.0 mM) conditions. (C) Alizarin staining in MOVAS-1 cells treated with CAY10566. ATF4-knockdown MOVAS-1 cells were treated with 300 nM CAY10566 for 7 days and stained with Alizarin red. (D) p-ATF4, total ATF4, and CHOP protein expression in ATF4-knockdown MOVAS-1 cells treated with CAY10566 for 30 min for p-ATF4 expression and for 6 h for other protein expression. GAPDH was used as a loading control. (E) Control and ATF4-knockdown MOVAS-1 cells were treated with CAY10566 (300 nM) for 12 h. Changes in gene expression are reported as ratios relative to the vehicle control. $^{*}P < 0.05$ versus control MOVAS-1 cells with vehicle. $^{\#}P < 0.05$ versus control MOVAS-1 cells with CAY10566. (F) ATF4 mRNA expression in MOVAS-1 cells treated with adenoviruses containing ATF4 (Ad-ATF4) or empty (Ad-empty) at a MOI of 40 for 6 h. (G) Mineralization and (H) ALP activity of VSMCs overexpressing ATF4. MOVAS-1 cells were treated with either Ad-ATF4 or Ad-empty for 6 h and then incubated for 7 days. (I) OCN mRNA levels were analyzed after 6 h of adenovirus treatment.

treatment was attenuated by the shRNA-mediated knockdown of Elovl6, which generates stearate from palmitate (Fig. 6J, K). These data suggest that the effects of palmitate on ATF4 expression are due to an increase in stearate. We also found that inhibition of acyl-CoA synthetase by triacsin C completely blocked the induction of ATF4 protein and CHOP mRNA expression induced by stearate treatment, accompanied with a reduction of mineralization and osteoblastic differentiation. This inhibition suggests that stearoyl-CoA or its downstream metabolite mediates the induction of ATF4 and ER stress. Stearoyl-CoA desaturase is an ER transmembrane enzyme that regulates the level of stearate in the ER by converting stearate to oleate (38, 39). CAY10566 is able to inhibit the activity of both SCD1 and SCD2, as SCD activity was undetectable in MOVAS-1 cells treated with 300 nM of CAY10566 treatment. Similar to stearate treatment, the treatment of MOVAS-1 cells with CAY10566 dose-dependently and potently induced p-PERK, p-eIF2α, ATF4, and CHOP protein expressions, which directly correlated with the reduction of SCD activity in MOVAS-1 cells. CAY10566 treatment also dose-dependently increased stearate levels in the ER of MOVAS-1 cells. In contrast to SCD inhibition, the overexpression of SCD1 completely attenuated ATF4 protein expression and mineralization induced by stearate treatment. In addition, PERK knockdown completely inhibited the induction of ATF4 expression by SCD inhibition and stearate (Fig. 6G and data not shown), suggesting that PERK senses stearate levels in the ER and activated the eIF2α-ATF4 signaling pathway. Because sXBP-1 mRNA levels were also increased in MOVAS-1 cells treated with stearate and CAY10566, other UPRs, such as the ATF6 and IRE-1 pathways, may also sense stearate levels in the ER. These pathways may contribute to stearate-induced vascular calcification, as it was recently reported that the IRE-1-XBP-1 pathway contributes to BMP-2-dependent vascular calcification by increasing Runx2 expression (40).

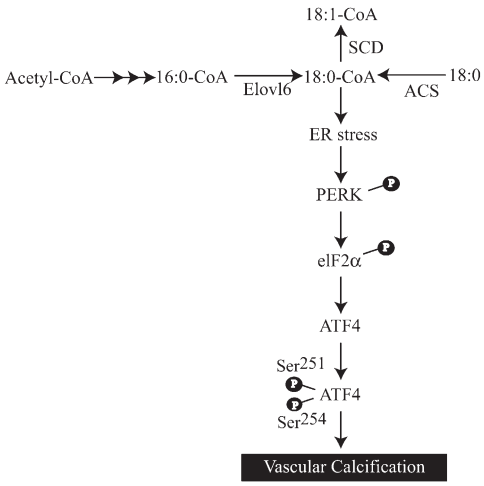

Fig. 9. Proposed mechanism by which stearate promotes vascular calcification. Palmitate (16:0), derived from lipoproteins and de novo lipogenesis, is elongated to stearate (18:0) in the ER. To induce ER stress, stearate has to be converted to the CoA-conjugated form. Stearoyl-CoA is incorporated into an ER membrane lipid, leading to ER stress that induces the expression of ATF4 through the activation of the PERK-eIF2α pathway. Activated ATF4 induces osteoblastic differentiation and mineralization in VSMCs.

The most striking result in our present study was that the knockdown of ATF4 expression by shRNA strongly alleviated osteoblastic differentiation and mineralization of MOVAS-1 cells induced by stearate and the SCD inhibitor. The residual calcific effect of these factors is probably due either to the remaining ATF4 activity in ATF4-knockdown MOVAS-1 cells or to other mechanisms contributing to osteoblastic differentiation and mineralization of MOVAS-1 cells. We also found that ATF4 overexpression induced osteoblastic differentiation and mineralization of MOVAS-1 cells. These findings provide insight into how stearate promotes vascular calcification.

The results of our current study establish a direct and important role for ATF4 in the regulation of vascular calcification induced by stearate and other factors, such as TNFα and oxidized lipids (data not shown). As summarized in **Fig. 9**, we propose that stearate-CoA or its metabolite activates the PERK-eIF2 pathway of UPR, which leads to the induction of ATF4 in VSMCs, which in turn induces osteoblastic differentiation and mineralization of VSMCs. Altogether, our results suggest that modulation of ATF4 transcriptional activity in VSMCs may be a promising strategy for preventing vascular calcification.

REFERENCES

1. Mizobuchi, M., D. Towler, and E. Slatopolsky. 2009. Vascular calcification: the killer of patients with chronic kidney disease. *J. Am. Soc. Nephrol.* **20:** 1453–1464.
2. Shanahan, C. M., M. H. Crouthamel, A. Kapustin, and C. M. Giachelli. 2011. Arterial calcification in chronic kidney disease: key roles for calcium and phosphate. *Circ. Res.* **109:** 697–711.
3. Li, X., H. Y. Yang, and C. M. Giachelli. 2006. Role of the sodium-dependent phosphate cotransporter, Pit-1, in vascular smooth muscle cell calcification. *Circ. Res.* **98:** 905–912.
4. Tintut, Y., J. Patel, F. Parhami, and L. L. Demer. 2000. Tumor necrosis factor-alpha promotes in vitro calcification of vascular cells via the cAMP pathway. *Circulation.* **102:** 2636–2642.
5. Luo, G., P. Ducy, M. D. McKee, G. J. Pinero, E. Loyer, R. R. Behringer, and G. Karsenty. 1997. Spontaneous calcification of arteries and cartilage in mice lacking matrix GLA protein. *Nature.* **386:** 78–81.
6. Boström, K., K. E. Watson, S. Horn, C. Wortham, I. M. Herman, and L. L. Demer. 1993. Bone morphogenetic protein expression in human atherosclerotic lesions. *J. Clin. Invest.* **91:** 1800–1809.
7. Watson, K. E., K. Boström, R. Ravindranath, T. Lam, B. Norton, and L. L. Demer. 1994. TGF-beta 1 and 25-hydroxycholesterol stimulate osteoblast-like vascular cells to calcify. *J. Clin. Invest.* **93:** 2106–2113.
8. Parhami, F., A. D. Morrow, J. Balucan, N. Leitinger, A. D. Watson, Y. Tintut, J. A. Berliner, and L. L. Demer. 1997. Lipid oxidation products have opposite effects on calcifying vascular cell and bone cell differentiation. A possible explanation for the paradox of arterial calcification in osteoporotic patients. *Arterioscler. Thromb. Vasc. Biol.* **17:** 680–687.
9. Hu, M. C., M. Shi, J. Zhang, H. Quinones, C. Griffith, M. Kuro-o, and O. W. Moe. 2011. Klotho deficiency causes vascular calcification in chronic kidney disease. *J. Am. Soc. Nephrol.* **22:** 124–136.
10. Kuro-o, M., Y. Matsumura, H. Aizawa, H. Kawaguchi, T. Suga, T. Utsugi, Y. Ohyama, M. Kurabayashi, T. Kaname, E. Kume, et al. 1997. Mutation of the mouse klotho gene leads to a syndrome resembling ageing. *Nature.* **390:** 45–51.
11. Miyazaki-Anzai, S., M. Levi, A. Kratzer, T. C. Ting, L. B. Lewis, and M. Miyazaki. 2010. FXR activation prevents the development of vascular calcification in ApoE$^{-/-}$ mice with chronic kidney disease. *Circ. Res.* **106:** 1807–1817.
12. Ting, T. C., S. Miyazaki-Anzai, M. Masuda, M. Levi, L. L. Demer, Y. Tintut, and M. Miyazaki. 2011. Increased lipogenesis and stearate accelerate vascular calcification in calcifying vascular cells. *J. Biol. Chem.* **286:** 23938–23949.
13. Geng, Y., J. J. Hsu, J. Lu, T. C. Ting, M. Miyazaki, L. L. Demer, and Y. Tintut. 2011. The role of cellular cholesterol metabolism in vascular cell calcification. *J. Biol. Chem.* **286:** 33701–33706.
14. Haze, K., H. Yoshida, H. Yanagi, T. Yura, and K. Mori. 1999. Mammalian transcription factor ATF6 is synthesized as a transmembrane protein and activated by proteolysis in response to endoplasmic reticulum stress. *Mol. Biol. Cell.* **10:** 3787–3799.
15. Ye, J., R. B. Rawson, R. Komuro, X. Chen, U. P. Dave, R. Prywes, M. S. Brown, and J. L. Goldstein. 2000. ER stress induces cleavage of membrane-bound ATF6 by the same proteases that process SREBPs. *Mol. Cell.* **6:** 1355–1364.
16. Harding, H. P., I. Novoa, Y. Zhang, H. Zeng, R. Wek, M. Schapira, and D. Ron. 2000. Regulated translation initiation controls stress-induced gene expression in mammalian cells. *Mol. Cell.* **6:** 1099–1108.
17. Kilberg, M. S., J. Shan, and N. Su. 2009. ATF4-dependent transcription mediates signaling of amino acid limitation. *Trends Endocrinol. Metab.* **20:** 436–443.
18. Yang, X., K. Matsuda, P. Bialek, S. Jacquot, H. C. Masuoka, T. Schinke, L. Li, S. Brancorsini, P. Sassone-Corsi, T. M. Townes, et al. 2004. ATF4 is a substrate of RSK2 and an essential regulator of osteoblast biology; implication for Coffin-Lowry Syndrome. *Cell.* **117:** 387–398.
19. Karsenty, G. 2008. Transcriptional control of skeletogenesis. *Annu. Rev. Genomics Hum. Genet.* **9:** 183–196.
20. Yu, S., R. T. Franceschi, M. Luo, J. Fan, D. Jiang, H. Cao, T. G. Kwon, Y. Lai, J. Zhang, K. Patrene, et al. 2009. Critical role of activating transcription factor 4 in the anabolic actions of parathyroid hormone in bone. *PLoS ONE.* **4:** e7583.
21. Xiao, G., D. Jiang, C. Ge, Z. Zhao, Y. Lai, H. Boules, M. Phimphilai, X. Yang, G. Karsenty, and R. T. Franceschi. 2005. Cooperative interactions between activating transcription factor 4 and Runx2/Cbfa1 stimulate osteoblast-specific osteocalcin gene expression. *J. Biol. Chem.* **280:** 30689–30696.
22. Yang, X., and G. Karsenty. 2004. ATF4, the osteoblast accumulation of which is determined post-translationally, can induce osteoblast-specific gene expression in non-osteoblastic cells. *J. Biol. Chem.* **279:** 47109–47114.
23. Saito, A., K. Ochiai, S. Kondo, K. Tsumagari, T. Murakami, D. R. Cavener, and K. Imaizumi. 2011. Endoplasmic reticulum stress response mediated by the PERK-eIF2(alpha)-ATF4 pathway is involved in osteoblast differentiation induced by BMP2. *J. Biol. Chem.* **286:** 4809–4818.
24. Mackenzie, N. C., D. Zhu, L. Longley, C. S. Patterson, S. Kommareddy, and V. E. MacRae. 2011. MOVAS-1 cell line: a new in vitro model of vascular calcification. *Int. J. Mol. Med.* **27:** 663–668.

25. Chalmers, J. A., S. Y. Lin, T. A. Martino, S. Arab, P. Liu, M. Husain, M. J. Sole, and D. D. Belsham. 2008. Diurnal profiling of neuroendocrine genes in murine heart, and shift in proopiomelanocortin gene expression with pressure-overload cardiac hypertrophy. *J. Mol. Endocrinol.* **41:** 117–124.
26. Watson, A. D., N. Leitinger, M. Navab, K. F. Faull, S. Horkko, J. L. Witztum, W. Palinski, D. Schwenke, R. G. Salomon, W. Sha, et al. 1997. Structural identification by mass spectrometry of oxidized phospholipids in minimally oxidized low density lipoprotein that induce monocyte/endothelial interactions and evidence for their presence in vivo. *J. Biol. Chem.* **272:** 13597–13607.
27. Flowers, M. T., M. P. Keller, Y. Choi, H. Lan, C. Kendziorski, J. M. Ntambi, and A. D. Attie. 2008. Liver gene expression analysis reveals endoplasmic reticulum stress and metabolic dysfunction in SCD1-deficient mice fed a very low-fat diet. *Physiol. Genomics.* **33:** 361–372.
28. Man, W. C., M. Miyazaki, K. Chu, and J. Ntambi. 2006. Colocalization of SCD1 and DGAT2: implying preference for endogenous monounsaturated fatty acids in triglyceride synthesis. *J. Lipid Res.* **47:** 1928–1939.
29. Hsu, J. J., J. Lu, M. S. Huang, Y. Geng, A. P. Sage, M. N. Bradley, P. Tontonoz, L. L. Demer, and Y. Tintut. 2009. T0901317, an LXR agonist, augments PKA-induced vascular cell calcification. *FEBS Lett.* **583:** 1344–1348.
30. Elefteriou, F., M. D. Benson, H. Sowa, M. Starbuck, X. Liu, D. Ron, L. F. Parada, and G. Karsenty. 2006. ATF4 mediation of NF1 functions in osteoblast reveals a nutritional basis for congenital skeletal dysplasiae. *Cell Metab.* **4:** 441–451.
31. Harding, H. P., Y. Zhang, H. Zeng, I. Novoa, P. D. Lu, M. Calfon, N. Sadri, C. Yun, B. Popko, R. Paules, et al. 2003. An integrated stress response regulates amino acid metabolism and resistance to oxidative stress. *Mol. Cell.* **11:** 619–633.
32. Elefteriou, F., J. D. Ahn, S. Takeda, M. Starbuck, X. Yang, X. Liu, H. Kondo, W. G. Richards, T. W. Bannon, M. Noda, et al. 2005. Leptin regulation of bone resorption by the sympathetic nervous system and CART. *Nature.* **434:** 514–520.
33. Cao, H., S. Yu, Z. Yao, D. L. Galson, Y. Jiang, X. Zhang, J. Fan, B. Lu, Y. Guan, M. Luo, et al. 2010. Activating transcription factor 4 regulates osteoclast differentiation in mice. *J. Clin. Invest.* **120:** 2755–2766.
34. Erbay, E., V. R. Babaev, J. R. Mayers, L. Makowski, K. N. Charles, M. E. Snitow, S. Fazio, M. M. Wiest, S. M. Watkins, M. F. Linton, et al. 2009. Reducing endoplasmic reticulum stress through a macrophage lipid chaperone alleviates atherosclerosis. *Nat. Med.* **15:** 1383–1391.
35. Borradaile, N. M., X. Han, J. D. Harp, S. E. Gale, D. S. Ory, and J. E. Schaffer. 2006. Disruption of endoplasmic reticulum structure and integrity in lipotoxic cell death. *J. Lipid Res.* **47:** 2726–2737.
36. Seimon, T. A., M. J. Nadolski, X. Liao, J. Magallon, M. Nguyen, N. T. Feric, M. L. Koschinsky, R. Harkewicz, J. L. Witztum, S. Tsimikas, et al. 2010. Atherogenic lipids and lipoproteins trigger CD36–TLR2-dependent apoptosis in macrophages undergoing endoplasmic reticulum stress. *Cell Metab.* **12:** 467–482.
37. Wei, Y., D. Wang, F. Topczewski, and M. J. Pagliassotti. 2006. Saturated fatty acids induce endoplasmic reticulum stress and apoptosis independently of ceramide in liver cells. *Am. J. Physiol. Endocrinol. Metab.* **291:** E275–E281.
38. Miyazaki, M., A. Dobrzyn, P. M. Elias, and J. M. Ntambi. 2005. Stearoyl-CoA desaturase-2 gene expression is required for lipid synthesis during early skin and liver development. *Proc. Natl. Acad. Sci. U S A.* **102:** 12501–12506.
39. Miyazaki, M., M. T. Flowers, H. Sampath, K. Chu, C. Otzelberger, X. Liu, and J. M. Ntambi. 2007. Hepatic stearoyl-CoA desaturase-1 deficiency protects mice from carbohydrate-induced adiposity and hepatic steatosis. *Cell Metab.* **6:** 484–496.
40. Byon, C. H., A. Javed, Q. Dai, J. C. Kappes, T. L. Clemens, V. M. Darley-Usmar, J. M. McDonald, and Y. Chen. 2008. Oxidative stress induces vascular calcification through modulation of the osteogenic transcription factor Runx2 by AKT signaling. *J. Biol. Chem.* **283:** 15319–15327.